Journal of Geophysical Research: Space Physics

RESEARCH ARTICLE
10.1029/2018JA025536

Key Points:
- Strong amplitude anomalies on NWC signal were observed during evening terminator time associated with the 17 March 2015 and the 25 June 2015 storms
- Stronger and longer duration signal amplitude anomalies occurred due to the March storm as compared to the June storm
- Wavelet analysis shows signature of AGWs/TIDs along the NWC Allahabad path associated with these storms

Correspondence to:
A. K. Maurya,
ajeet.iig@gmail.com

Citation:
Maurya, A. K., Venkatesham, K., Kumar, S., Singh, R., Tiwari, P., & Singh, A. K. (2018). Effects of St. Patrick's Day geomagnetic storm of March 2015 and of June 2015 on low-equatorial *D* region ionosphere. *Journal of Geophysical Research: Space Physics*, *123*, 6836–6850. https://doi.org/10.1029/2018JA025536

Received 30 MAR 2018
Accepted 21 JUL 2018
Accepted article online 4 AUG 2018
Published online 21 AUG 2018

Effects of St. Patrick's Day Geomagnetic Storm of March 2015 and of June 2015 on Low-Equatorial *D* Region Ionosphere

Ajeet K. Maurya[1], K. Venkatesham[2], Sushil Kumar[3], Rajesh Singh[2], Prabhakar Tiwari[2], and Abhay K. Singh[4]

[1]Department of Physics, Doon University, Dehradun, India, [2]Dr. K S K Geomagnetic Research Laboratory, IIG, Allahabad, India, [3]School of Engineering and Physics, University of the South Pacific, Suva, Fiji, [4]Atmospheric Physics Lab, Department of Physics, Banaras Hindu University, Varanasi, India

Abstract *D* region effects of the 17–19 March 2015, a St Patrick's Day super geomagnetic storm ($Dst = -223$ nT), using a navigational transmitter very low frequency (VLF) signal (NWC, 19.8 kHz) recorded at a low-latitude Indian station, Allahabad (geomag. lat., 16.45°N), have been analyzed and compared with similar strength of the 22–25 June 2015 storm ($Dst = -204$ nT). During the March storm, NWC signal amplitude decreased on 17 March (main phase of the storm) and recovered on 27 March, which is 1 day after the recovery of the storm, whereas for the June storm, VLF amplitude decreased for 2 days only during its recovery phase. The decrease in the amplitude was pronounced during evening terminator for both the storms. The modeling of VLF signal anomaly on 17 March and on 25 June using Long-Wave Propagation Capability code shows an increase in the *D* region reference height (h') by ~2.6 km and ~2.5 km, for March and June storms, respectively. The *D* region electron density (N_e) determined using storm time h' and sharpness factor β shows a decrease in the N_e during the main phase followed by a slow recovery during the recovery phase of the March storm, whereas June 2015 storm showed a decrease in the N_e only on 25 and 26 June. Morlet Wavelet analysis of the amplitude for both the storms shows a presence of strong wave-like signatures, suggesting propagation of atmospheric gravity waves/traveling ionosphere disturbances to the low latitude *D* region due to the Joule heating at high latitudes.

1. Introduction

The *D* region (~60–90 km altitude), a lower part of the ionosphere, is highly useful for the extremely low frequency (ELF) and the very low frequency (VLF) radio wave propagation, navigation, and submarine communication (Barr et al., 2000). This region can be affected by severe space and terrestrial weather conditions (Kumar et al., 2015; Kumar et al., 2017; Maurya et al., 2012; Peter et al., 2006; Thomson et al., 2004; Thomson et al., 2005). Despite the important role of the *D* region of ionosphere, it remained relatively unexplored due to its low electron density which hinders use of the traditional techniques (e.g., Ionosonde, Global Positioning System [GPS], and Radars) from its probing but can be studied by using ELF and VLF radio waves (Cummer & Inan, 2000). VLF (3–30 kHz) waves generated by lightning discharges and powerful VLF navigational transmitters are reflected from the lower ionosphere (*D* region) and Earth's surface and can travel very long distances in the Earth-ionosphere waveguide with a very little attenuation. This property makes VLF waves as one of the most reliable tools to study the *D* region in the height range of ~60–90 km (Hargreaves, 1992).

The solar flares and geomagnetic storms are two major space weather phenomena with former affecting the entire daytime ionosphere and later mainly the high-latitude ionosphere with their effects propagating towards the lower latitudes (Kumar et al., 2015). The *D* region response to solar flares has been well studied by several previous workers (e.g., Thomson et al., 2005; Grubor et al., 2005; Selvakumaran et al., 2015), which increases sudden ionization, but the geomagnetic storm effect mainly occurs in the high and midlatitude *D* region due to energetic electron precipitation (EEP) that causes localized electron density enhancements (Clilverd et al., 2010; Kikuchi & Evans, 1983; Peter et al., 2006; Rodger et al., 2007). The geomagnetic storm effect on the *D* region particularly at low and equatorial latitudes still remains not well known despite few recent efforts (e.g., Choudhury et al., 2015; Kumar et al., 2015). In the past, few attempts were made to study storm effects on the *D* region by using VLF observations at middle- and high-latitude stations (Araki, 1974; Kikuchi & Evans, 1983; Kleimenova et al., 2004). Kleimenova et al. (2004) reported negative phase and

amplitude changes (also called negative storm effect on VLF subionospheric propagation) in the day and more pronounced effect at the night for low and midlatitudes (Australia-Kamchatka radio path). Choudhury et al. (2015) analyzed *D*-layer preparation time depth during long-duration (>20 hr) geomagnetic storms on the NWC signal recorded at Agartala (23.75°N, 91.25°E), India, during November 2008 to November 2011. They found negative correlation between *D*-layer preparation time depth and geomagnetic disturbance index (A_P) based on eight cases of long duration geomagnetic storms. The geomagnetic storm associated *D* region changes during major to severe geomagnetic storms particularly at low latitudes still remain unknown and warrant further studies.

The year 2015 was the year of peak solar activity during solar cycle 24. There occurred two strongest and almost same intensity geomagnetic storms. The first storm called the St. Patrick's Day geomagnetic storm of 17 March 2015 was the most severe (min *Dst* = −223 nT) storm of current solar cycle 24. The interplanetary origin of this St. Patrick's Day storm and its consequences on the Earth's *F* and *E* regions of ionosphere and magnetosphere is one of the most studied space weather events of solar cycle 24 with most articles published under JGR-Space Physics special collection on "Geospace system responses to the St. Patrick's Day storms in 2013 and 2015" (Zhang et al., 2017). Astafyeva et al. (2015) presented a global ionospheric response of this storm using multi-instrument (GPS receiver, Ionosonde, and Satellite) observations. They reported a complex storm effect which varied with longitude and hemisphere. Both positive (increase) and negative (decrease) in the electron density and the total electron content (TEC) associated with this storm were observed. Analyzing the global and regional electron content (GEC and REC) data, Nava et al. (2016) analyzed the effect of St. Patrick's day storm at middle and low latitudes in the global longitudinal sector and observed positive storm effect during the main phase of the storm and long-lasting negative effect during the recovery phase. Ray et al. (2017) studied TEC and amplitude and phase scintillations at different GPS stations in the Indian sector along with the occurrence of global equatorial spread-F using total ion density drift measurements from Communication and Navigation Outage Forecast System satellite during 17–19 March 2015 storm and found TEC enhancements along 77°E around 10:00 UT and intense scintillation during 15:00–16:00 UT on 17 March as compared to those on 16 and 18 March. There are several other papers on upper ionospheric effects of this storm under "JGR-Space Physics special collection," but none talks about the *D* region effects of this storm. The second strongest storm occurred on 22 June 2015 having minimum *Dst* value of −204 nT. This storm has not been studied in details as was St. Patrick's Day storm, but there are few publications on June 2015 storm effects mostly on the *E* and *F* regions of the ionosphere. Astafyeva et al. (2016) studied the ionospheric effect of 22–25 June 2015 storm using the TEC data from Swarm satellite constellation. They have observed negative ionospheric storm in the day during initial and main phase owing to storm time penetration of high-latitude electric field.

The 2015 storms (St. Patrick's Day storm of 17 March and 22 June, hereafter named as March storm and June storm, respectively) provided us with an opportunity to investigate storm effect on the NWC subionospheric VLF signal propagation and on the *D* region over low-equatorial latitudes which for these storms have not been studied so far. In this work we have analyzed diurnal variation of NWC (19.8 kHz) VLF transmitter signal recorded at an Indian low-latitude station, Allahabad (25.41°N, 81.93°E), during these storms. The NWC signal propagation path extending from its low-latitude location in Australia to a low-latitude station in the Indian sector through a trans-equatorial path is shown in Figure 1. The NWC VLF transmitter signal showed an amplitude decrease (anomaly) during the main phase of March storm during sunset terminator times and thereafter for several days during its recovery phase, whereas for the June storm the amplitude anomaly is seen only on 25 and 26 June during its recovery phase. Long-Wavelength Propagation Capability (LWPC) code has been utilized to model VLF signal anomalies to find the *D* region changes associated with these storms. Morlet wavelet analysis of NWC VLF signal amplitude has been carried out to identify any wave-like signatures (WLS) due to atmospheric gravity waves (AGWs) associated with these storms which could be the manifestations of traveling ionospheric disturbances (TIDs) from high to low latitudes.

2. Data Analysis and Modeling

The VLF data are routinely recorded with Stanford University developed Automatic Weather Electromagnetic System for Observation Modeling and Education (AWESOME) VLF receiver (Cohen et al., 2010; Singh et al., 2010) installed at a quiet location near Allahabad (geog. lat. 25.41°N, long. 81.93°E; geomag. lat. 16.45°N, long.

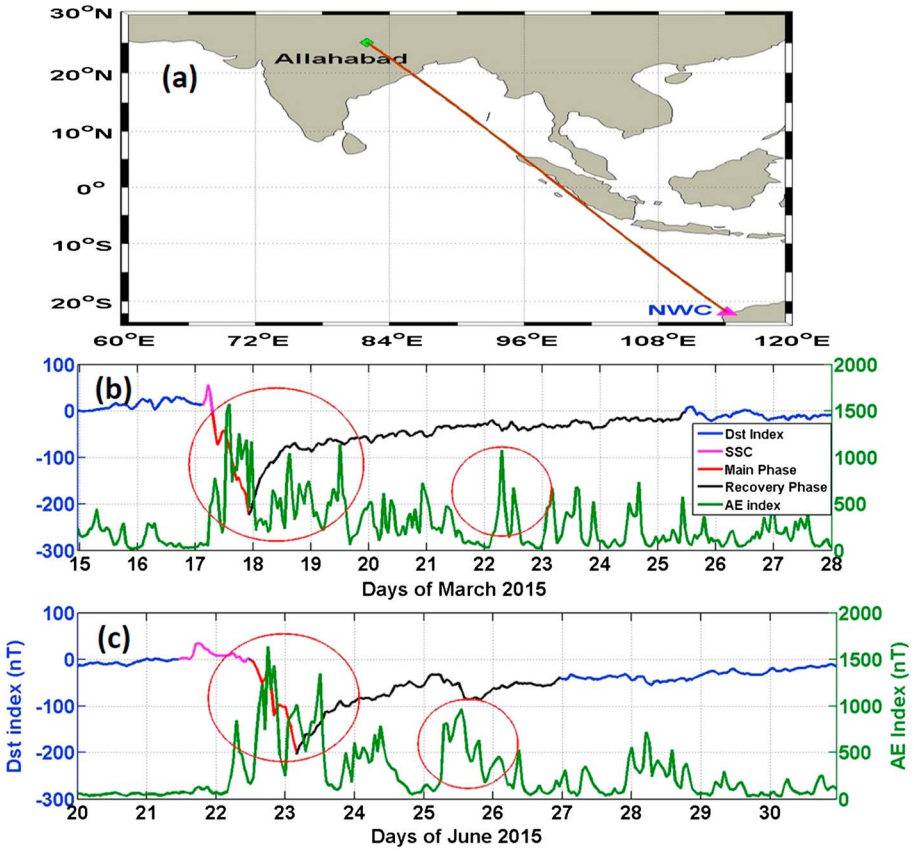

Figure 1. (a) The map showing receiving station, Allahabad, NWC (19.8 kHz) very low frequency transmitter locations, at low-latitude locations. Variation of *Dst* index (primary *y* axis) and auroral electrojet (*AE*) index (secondary *y* axis) (b) from 15 to 28 March 2015 and (c) from 20 to 30 June 2015. The region with the red circles indicates large (~1,000 nT) variation of *AE* index.

153.70°E), India. The data are recorded at high resolution (50 Hz), but here we have used 1-min average data for the analysis. The map showing location of Allahabad (ALD) station, NWC (19.8 kHz, geog. lat. 21.82°S; geog. long. 114.17°E) VLF transmitter along with their Transmitter Receiver Great Circle Path (TRGCPs) is shown in Figure 1a. The TRGCP path length for NWC-ALD path is ~6,300 km. The ionosonde data used to extract information about *F* region variations during the March and June 2015 geomagnetic storms are obtained from the same Allahabad site where Canadian Advanced Digital Ionosonde is in operation.

The St. Patrick's Day geomagnetic storm of 2015 (March storm) began approximately at 04:45 UT on 17 March, when a double-halo CME hit the Earth's magnetic field. Initially, Interplanetary Magnetic Fiend (IMF) B_z component went northward reaching ~27 nT for a while, giving storm sudden commencement before it turned southward until about 06:00 UT. The storm reached its peak (severe) intensity at ~00:00 UT on 18 March with minimum *Dst* ~ −223 nT and recovered on 25 March. The variation of *Dst* index during different stages of this storm is presented in Figure 1b, wherein the magenta color represents storm sudden commencement, the red color main phase, and the black color the recovery phase of the storm. The secondary *y* axis of Figure 1b shows the variation of auroral electrojet (*AE*) index during this storm. The variation of interplanetary parameters and geomagnetic conditions for this storm can be found in many previous works (e.g., Marubashi et al., 2016; Ramsingh et al., 2015; Verkhoglyadova et al., 2016; Wu et al., 2016). The June 2015 storm began with two CMEs hitting the Earth at ~5:45 UT and ~18:38 UT on 22 June 2015. The solar speed increased from ~450 to ~700 km/s and pressure from 7 to 55 nPa. The IMF B_z fluctuated from southward/northward from ~19:20 UT on 22 June to ~08 UT on 23 June. It remained southward for longest duration from 08 UT to 12 UT on 23 June 2015, which caused minimum *Dst* of ~−204 nT at ~4:30 UT on 23 June 2015. Figure 1c shows *Dst* variation for the June storm with different colors representing different stages of the storm, and the variation of *AE* index is shown on the

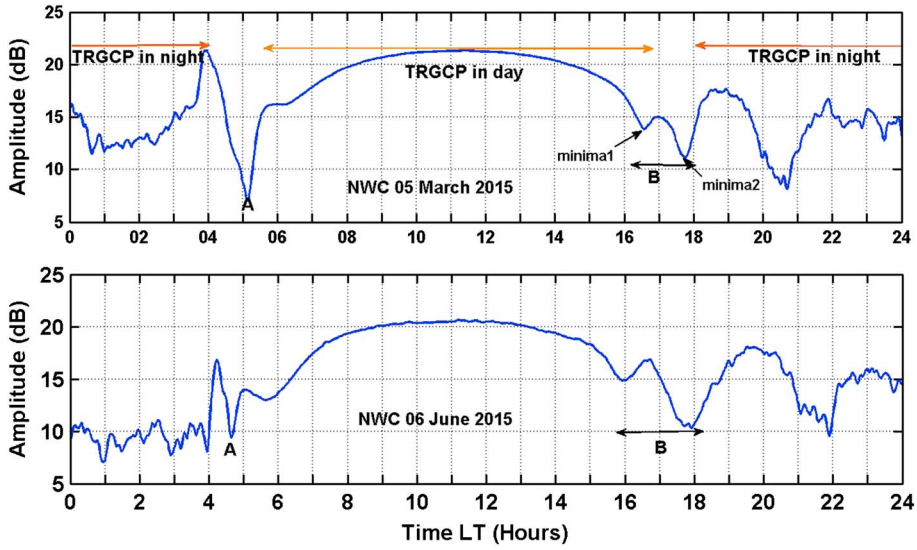

Figure 2. A sample record of NWC (19.8 kHz) very low frequency signal amplitude at Allahabad on (top) 5 March 2015 and (bottom) 6 June 2015. Points A and B are during the sunrise and sunset terminator, respectively. minima1 and minima2 are the first and second minima during sunset terminator taken as reference point for the analysis.

secondary *y* axis. More details on the June 2015 storm and interplanetary conditions can be found in previous works (e.g., Astafyeva et al., 2016, 2018).

A sample record of diurnal variation of NWC VLF signal amplitude at Allahabad on geomagnetically quiet days, 5 March 2015 and 6 June 2015, is presented in Figure 2. Figure 2 shows two typical minima (marked as A and B), called "sunrise" and "sunset" minima or "terminator time," which are generated due to the modal interference (Clilverd et al., 1999). In the evening (near point B), two minima appear close to each other with first minima (minima1) having higher amplitude compared to second (minima2). We have used 12-day VLF data for the March storm during 16–27 March 2015 and 8-day data for the June storm from 20 to 28 June 2015; there is a data gap of 1 day for 21 June. We have not utilized phase data for the analysis because most of the time NWC signal phase is not good enough to be useful for the analysis. We do have 1 day (17 March) of good NWC phase data, which has been used to determine the *D* region changes associated with the March storm.

To estimate the storm time *D* region changes we have used LWPC v2.1code developed by U.S. Navy (Ferguson, 1998). LWPC is a versatile code which accepts model solution of wave propagation and treats Earth-ionosphere waveguide as a parallel plate with the ground as imperfect conductor and lower ionosphere as anisotropic magnetized collisional plasma. LWPC code divides the entire path length between transmitter and receiver into segments with same characteristic parameters (Wait & Spies, 1964) that are reference height h' (in km) and electron density gradients characterized by the sharpness factor β (in km^{-1}). The VLF wave electric field is calculated sequentially in each segment with the user defined ground conductivity and permittivity. The model *D* region electron density N_e (*z*) as a function of altitude *z* is given by the following equation:

$$N_e(z) = 1.43\times10^7\left[\exp\left(-0.15h'\right)\exp(\beta-0.15)\left(z-h'\right)\right]\ \mathrm{cm}^{-3} \quad (1)$$

The electron-neutral collision frequency υ_e (*z*) (per second s^{-1}) is given by the following expression:

$$v_e(z) = 1.816\times10^{11}\exp(-0.15z)\mathrm{s}^{-1} \quad (2)$$

The υ_e (*z*) varies with altitude exponentially and decreases with increase in the altitude (Ferguson, 1998). Equation (1) has been widely used by researchers to estimate the N_e (*z*), which is valid up to 100 km altitude (e.g., Maurya et al., 2012; Thomson et al., 2014).

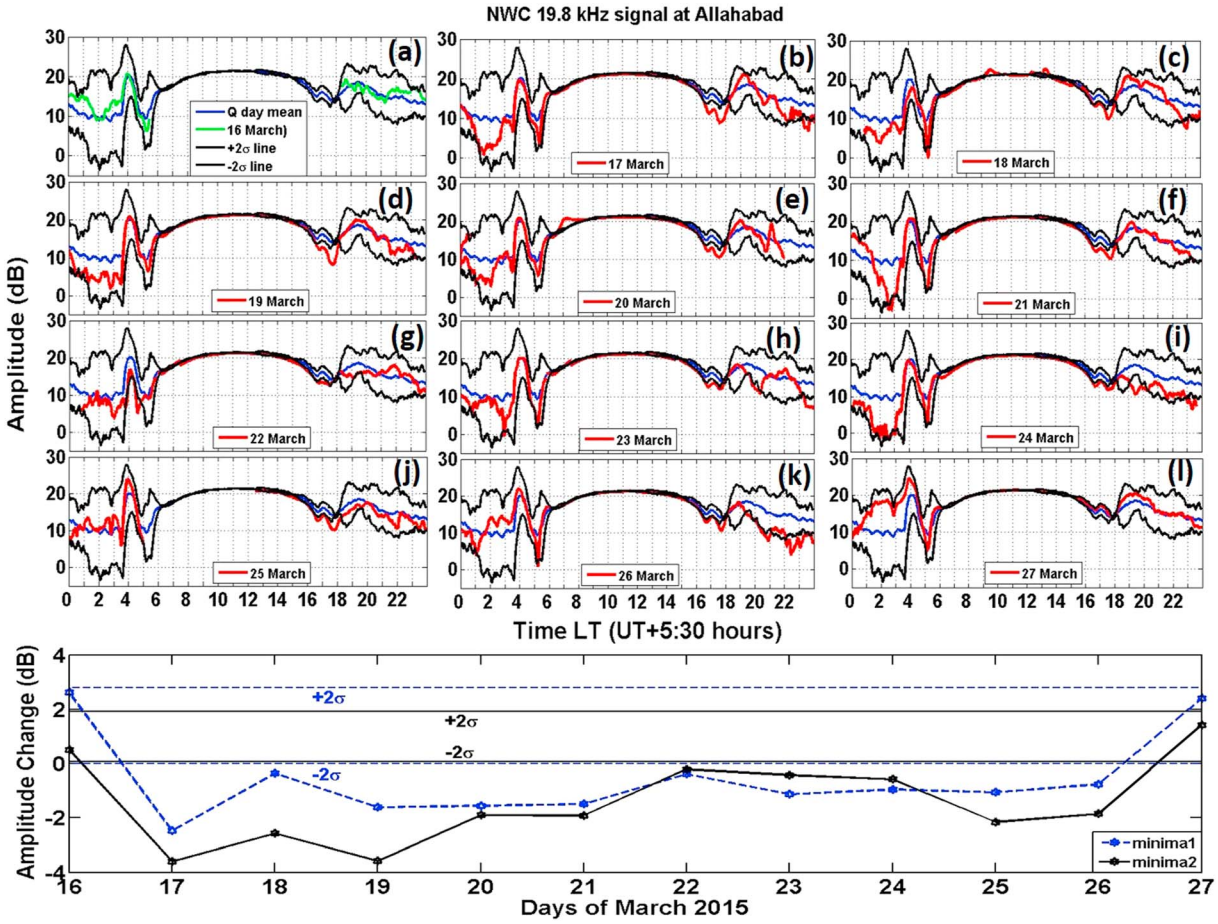

Figure 3. (a–i; top) NWC very low frequency signal amplitude variation during 16–27 March 2015 which covers days before storm, day of storm main phase onset, and storm recovery and post recovery days. The average amplitude variation on five international quiet days (blue line) along with ±2σ line (black line) are also shown in the upper panel. (bottom) The amplitude anomalies (difference between signal change and −2σ line) for NWC signal estimated from five quiet day amplitude mean and each day amplitude during 16–27 March 2015 corresponding to minima1 (blue) and minima2 (black). The region between two horizontal lines (black and blue) (marked as ±2σ lines) represents the variation in normal days amplitude due to day-to-day variability with 95% confidence limit for minima1 and minima2, respectively.

3. Results

3.1. NWC VLF Signal Analysis During the St Patrick's Day Storm: 17–18 March 2015

To determine St Patrick's Day (17–19 March 2015) storm effect on VLF subionospheric propagation, we have used NWC (19.8 kHz) VLF transmitter signals recorded at a low-latitude station, Allahabad, India. The upper panel of Figures 3a–3i shows diurnal variation of NWC amplitude during 16–27 March 2015 which includes a day before the storm (16 March), a day during the storm main phase (17 March), 8 days during the recovery phase (18–25 March), and 2 day after the recovery phase (26 and 27 March). The blue line represents the average amplitude variation on five international quiet (*Q*) days (the details about which could be found on the following Web link: http://isgi.unistra.fr/events_qdays.php) which is considered as unperturbed or normal day VLF signal variation. The green line represents VLF signal variation on a day (16 March) before storm, and the red line represents signal amplitude during the storm main phase (17 March) and the recovery phase and after recovery days (18–27 March) of the storm. The black gray curves are *Q* time signal amplitude ± 2σ(*t*), where σ is the standard deviation. Any change in the signal amplitude during the storm from normal signal value (average on *Q* days) ±2σ line is considered as signal anomaly due to this geomagnetic storm with 95% confidence. As seen in Figure 3, there is a significant decrease (below −2σ line; two minima) near evening terminator (ET) which is consistent throughout the storm period; hence, we have used two minima during ET transition referred to as minima1 and minima2 as reference points to determine storm effect on the

VLF subionospheric propagation and hence on the *D* region. Further, the significant decrease (below -2σ line) in morning terminator (point A) is only seen on 18 and 26 March, which may not be associated with storm. Therefore, we have not used morning terminator (point A) in the present analysis. As shown in the Figure 3a (upper panel), on 16 March (a day before the storm), the NWC VLF signal amplitude varied within $\pm2\sigma$ lines estimated from five *Q* days mean signal level variation, whereas on the storm main phase day (17 March, Figure 3b; upper panel) around ~16:30 LT, the signal amplitude began decreasing below -2σ and remained low for ~2 hr and then approached -2σ line after ~18:30 LT. The decrease in the signal amplitude at minima1 and minima2 is ~2.50 and 3.60 dB, respectively, with reference to -2σ line. On 18 March (Figure 3c, upper panel), there can be seen at three instances when signal amplitude crossed $+2\sigma$ line during the daytime (06–16 LT) which is due to the class C solar flares. Due to C5.5 class flare at 16:00 LT, the amplitude decrease near minima1 and minima2 is less in amount and duration as compared to that on 17 March. On 19 March (Figure 3d, upper panel), the decrease in the amplitude near ET occurred of same duration as on 17 March but with the decreased magnitude (~1.60 and 3.58 dB, respectively, for minima1 and minima2). In Figure 3e (on 20 March) we have another C7.9 flare event at around 7 LT. During recovery phase, decrease in the amplitude near ET recovered with the progress of the recovery phase (18–26 March; Figures 3g–3i, upper panel). On 27 March amplitude recovered completely and was within $\pm2\sigma$ line throughout the period. It is interesting to note that there were few instances, especially during the night hours of TRGCP, when NWC signal was below -2σ line (e.g., 17 March between 23 and 24 LT, 18 March between ~22 and 23 LT, 21 March between ~2 and 3 LT, on 23 March and 24 March between 23 and 24 LT, and on 26 March between ~21 and 23 LT). The amplitude decreases (anomalies) are most probably because of nighttime *D* region large day-to-day variability that makes it difficult to determine whether signal anomalies are of storm generated (e.g., Maurya et al., 2012; Ohya et al., 2011). Hence, such nighttime signal changes have not been included in the analysis. Thus, the most consistent decrease in the amplitude was observed between ~16:30 LT and 18:00 LT. Overall the storm effect lasted for about 10 days and such long-lasting storm effect is called as "storm after effect" (Bolerose & Thomas, 1968).

The NWC signal anomalies below -2σ line corresponding to minima1 and minima2 (presented in blue and black colors, respectively) during 16–27 March are given in Figure 3 (bottom) wherein $\pm2\sigma$ lines represent the region of amplitude change corresponding to minima1 (blue lines) and minima2 (black lines) which could be due to day-to-day variability and the region below and above these lines define signal anomaly due to this storm with 95% confidence limit. As seen from Figure 3 (bottom), amplitude variation was normal on 16 March and maximum decrease (anomaly) in the signal amplitude occurred on the storm main phase day (17 March) which recovered on the following days with progress of the storm recovery phase and became normal by 27 March.

In order to estimate the *D* region ionospheric changes associated with signal anomalies, we have used LWPC V 2.1 code. The LWPC code is widely used by researchers to estimate *D* region changes due to various geophysical and space weather phenomena such as solar eclipse, solar flares, and geomagnetic storms (Clilverd et al., 2001; Kumar et al., 2015; Maurya et al., 2014; Thomson & McRae, 2009). Since pronounced storm effect was seen near ET, we have modeled VLF signal anomalies near the terminator at the time of minima1 and minima2. It is important to note that VLF signal modeling during terminator transition is difficult as one has to apply LWPC for a path having sections both in day and night simultaneously. Further, as the magnitude of observed VLF signal (amplitude and phase recorded using AWESOME VLF receiver) is lower than that estimated from LWPC modeling of NWC signal, the values of amplitude of 35.6 dB and phase of 15° were added respectively to NWC signals strength, to calibrate the observed signal values.

The following method has been adopted for LWPC simulations: We selected a quiet day (5 March) of March month and run LWPC V2.1 code at the time of minima1 (11:04 UT). The solar zenith angle variation (by calculating solar terminator speed) along great circle path is incorporated into RANGE subprogram of LWPC code. We have assumed that the β and h' along the path are constant during day and night and vary sharply near terminator as discussed by Chakraborty et al. (2017). We obtained sets of h' and β values for different segments of the path which we averaged them to get the normal time set of h'=82.7 km and β = 0.33 km^{-1} which gives normal time NWC amplitude and phase of 13.83 dB and $-58.12°$ at minima1. On 17 March (storm main phase) we have both good amplitude and phase data for NWC signal (Figure 3b) with amplitude and phase anomaly of -2.80 dB and 44.58° at the time of minima1. The normal values of h' and β were

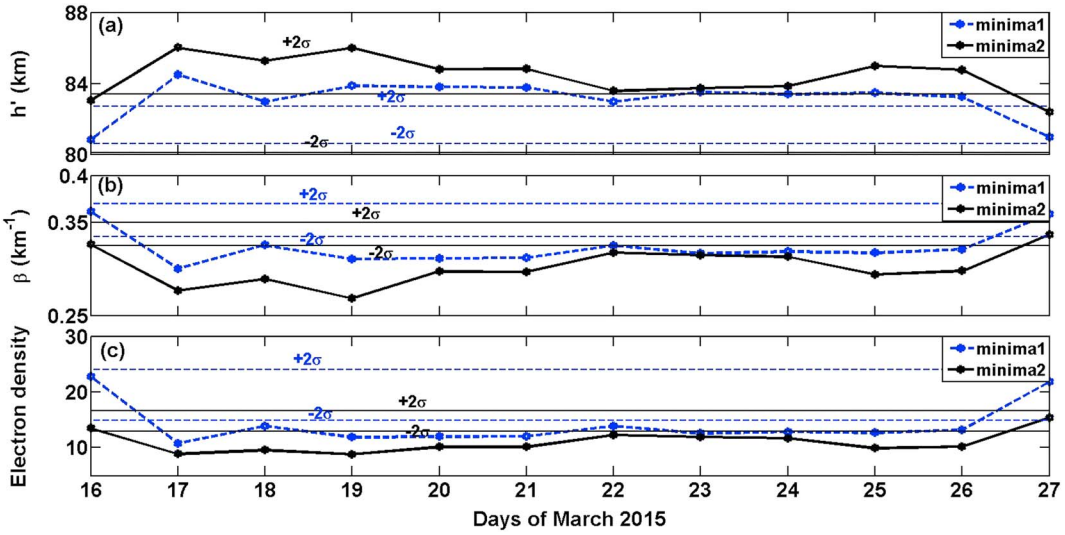

Figure 4. The variation of Wait's lower ionospheric parameters: (a) the reference height (h' in km) and (b) the electron density gradient (β in km^{-1}) during 16–27 March 2015 for NWC signal at minima1 (blue) and minima2 (black). (c) The electron density variation during 16–27 March 2015 at an altitude of 75 km (daytime reference altitude) at minima1 (blue) and minima2 (black).

changed in steps of 0.1 km and 0.01 km^{-1}, respectively, to obtain the LWPC output to match normal time LWPC amplitude and phase plus signal anomaly (amplitude and phase). The storm time disturbed values of h' and β at the minima1 time of 11:22 UT on 17 March were estimated h' = 84.5 km and β = 0.30 km^{-1}, which shows an increase in h' by1.8 km and a decrease in β of 0.03 km^{-1} with uncertainty of 0.1 km in h' and 0.01 km^{-1} in β. These changes in h' and β are not the changes during the ET time only rather are average change along the entire path that will produce same anomalies at the time of minima1. Similarly, at minima2, the normal time h'=83.4 km and β = 0.32 km^{-1} were obtained and corresponding amplitude and phase values were 12.33 dB and 124.6°. The anomalies in the signal amplitude and phase at minima2 were −3.85 dB and 10°. The values of h' and β on 17 March (storm day) at the minima2 time of 12:05 UT were obtained as h' = 86.0 km and β = 0.28 km^{-1}, which shows an increase in h' of 2.6 km and a decrease in β of 0.04 km^{-1}. We do not have usable phase data on many other days apart from that on 17 March, so we cannot directly use LWPC for the estimation of disturbed values h' and β for other days. To solve this difficulty, we devised a method to estimate disturbed values of h' and β for the rest of the days used in the analysis. An amplitude perturbation of 2.80 dB on 17 March gave change in h' and β values by +1.80 km and −0.03 km^{-1}, respectively. Hence, change in h' and β values corresponding to 1 dB decrease in the amplitude gives ~0.6 km increase in $h'$and ~0.01 km^{-1} decrease in β, which is the same for both minima1 and minima2. By using this method, we estimated $h'$and β values for signal anomalies on the remaining days, and the results are given in Figures 4a and 4b. We call this as "method2," which provides approximate results but serves the purpose in absence of phase data. Similar method was first proposed by Clilverd et al. (2001) to model the *D* region effects of 11 August 1999 total solar eclipse for short paths using VLF transmitter signal observations in Europe and had also been used by other workers in absence of good phase data (Guha et al., 2012; Phanikumar et al., 2014).

As shown in Figure 4a, the increase in $h'$was maximum on 17 March (storm main phase), which recovered during the recovery phase of the storm until 27 March but β showed opposite trend (Figure 4b) to that of h'. The values of $h'$and β for minima2 (black color) showed almost same variation as that for minima1, except that $h'$was higher and β was lower for minima2 compared to minima1. We have also estimated *D* region N_e (z) by using $h'$and β as input for equation (1) at 75 km altitude (standard *D* region altitude during terminator time) which is shown in Figure 4c for minima1 (blue) and minima2 (black). The N_e (*z*) was minimum on 17 March, which gradually recovered toward normal level. The N_e (*z*) was slightly lower for minima2 compared to minima1; this is obvious because minima2 is more toward nightside as compared to minima1.

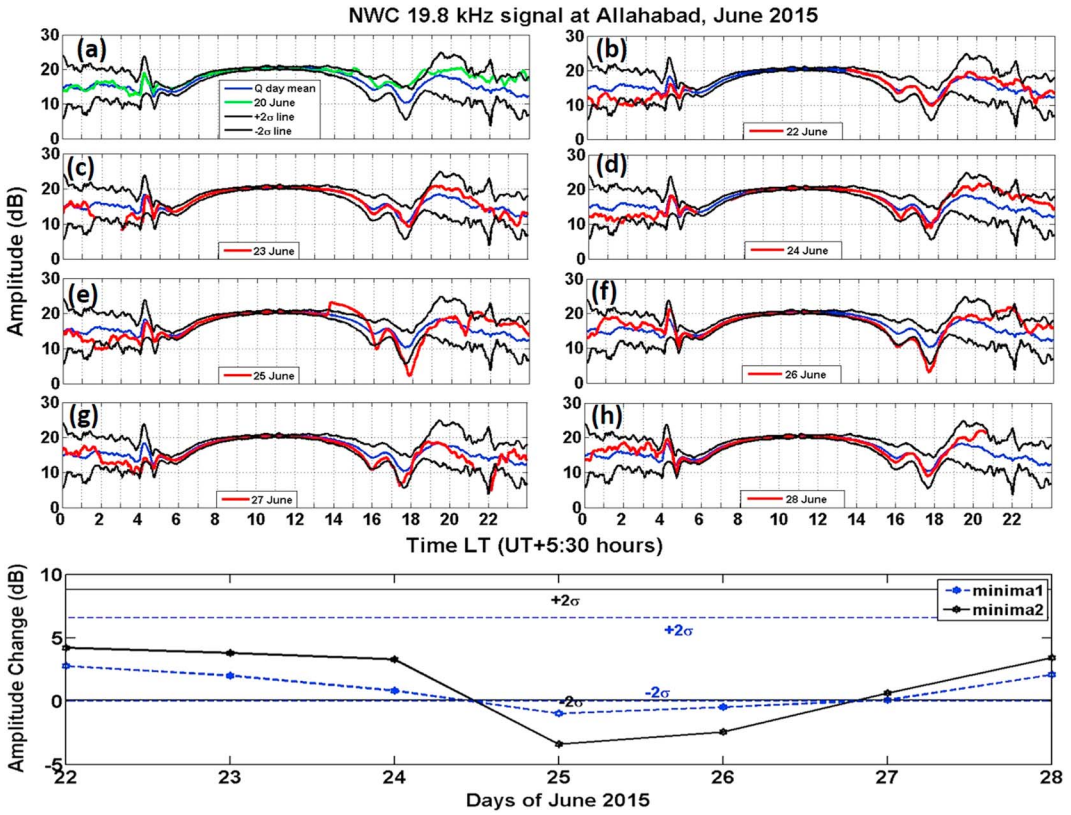

Figure 5. Similar to Figure 3 but for June 2015 storm.

3.2. NWC VLF Signal Analysis During the 22–25 June 2015 Storm

Figures 5a–5h (upper panel; similar as Figure 3, upper panel) show the NWC signal amplitude variation, before, during, and after the main phase of the June storm. There was no change in the amplitude on 20 June (a normal day; Figure 5a, upper panel) from mean level. Starting from storm main phase (22–23 June 2015; Figures 5b and 5c, upper panel) and on 24 June (Figure 5d, upper panel) we did not observe any amplitude change as it remained between ±2σ lines throughout the storm period. On 25 June (Figure 5e, upper panel) the amplitude decreased by ~1 and 3.4 dB at mimima1 and minima2, respectively. Interestingly, amplitude decrease (below −2σ line) is only seen at minima1 and minima2. The increase in VLF signal amplitude (above +2σ line) at ~13:46 LT is due to solar flare of class M7.9. Further, on 26 June (Figure 5f, upper panel), the signal amplitude decreased by ~0.5 and ~2.5 dB at minima1 and minima2, respectively. On 27 and 28 June, the signal amplitude showed normal day variation, indicating full recovery of the storm effect. The NWC signal also showed amplitude decrease below −2σ line on 22 June and 25 June between 1:30 LT to 2:30 LT, and above +2σ line on 25 June and 26 June between 21 and 22 LT. These variations are most probably due to large nighttime *D* region variability because of longer path length. Therefore, it is difficult to determine any significant amplitude change at the nighttime associated with the storm. Figure 5 (bottom panel) shows the measured decrease in the NWC signal amplitude on each day during the June storm period (22–28 June 2015) at minima1 (blue color, dotted line) and minima2 (black color, solid line). A decrease in the amplitude of NWC signal due to the June storm was observed on 25 and 26 June near ET at minima1 and minima2 during recovery phase of storm, whereas for the March storm the amplitude decrease was observed starting from main phase of storm till the full recovery of storm.

To estimate 22–25 June storm effect on *D* region over low equatorial latitude path, we have used LWPC modeling in the same way as done for March storm in section 3.1. We found normal day (selected quite day of 6 June) $h'$and β values of 83.06 km and 0.28 km^{-1}, and 85.75 km and 0.27 km^{-1}, at minima1 and minima2, respectively. The perturbed values of $h'$and β corresponding to the signal anomaly on 25 June are obtained h' = ~83.77 km and β = 0.26 km^{-1} for minima1 and h' = ~88.21 km and β = 0.23 km^{-1} for minima2 and for 26

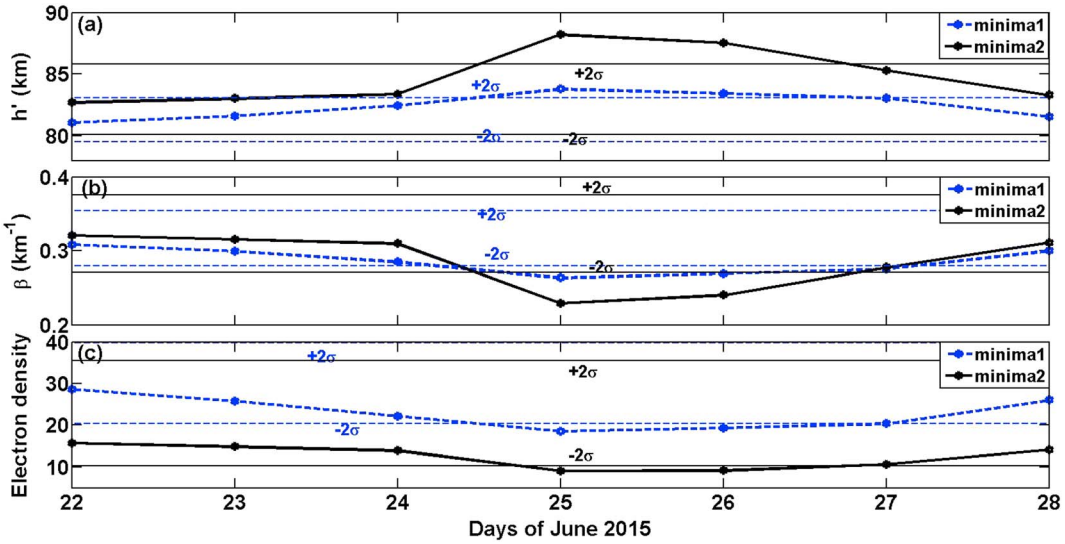

Figure 6. Similar to Figure 4 but for June 2015 storm.

June are h' = ~83.42 km and β = 0.27 km^{-1} for minima1 and h' = ~87.52 km and β = 0.24 km^{-1} for minima2. Further, we have also estimated perturbed h' and β values on each day at minima1 and minima2 during storm, and results are presented in Figures 6a and 6b. As shown in Figures 6a and 6b, the maximum perturbation in h' and β occurred on 25 June. Using equation (1), we estimated storm time D region N_e (z) at 75 km altitude for low-latitude path as presented in Figure 6c, which clearly shows a decrease in N_e on 25 June and 26 June with gradual recovery toward normal level on 27 June.

In order to verify our LWPC modeling results and corresponding h' and β values for normal day and storm day, we have reproduced amplitude of NWC signal of mean Q days and storm days for both the storms by inputting estimated h' and β values in the LWPC code and run the LWPC at every 15 min. The results are shown in Figure 7 for 17 March and 26 June for the period 4 LT to 18:30 LT, which covers morning and ET

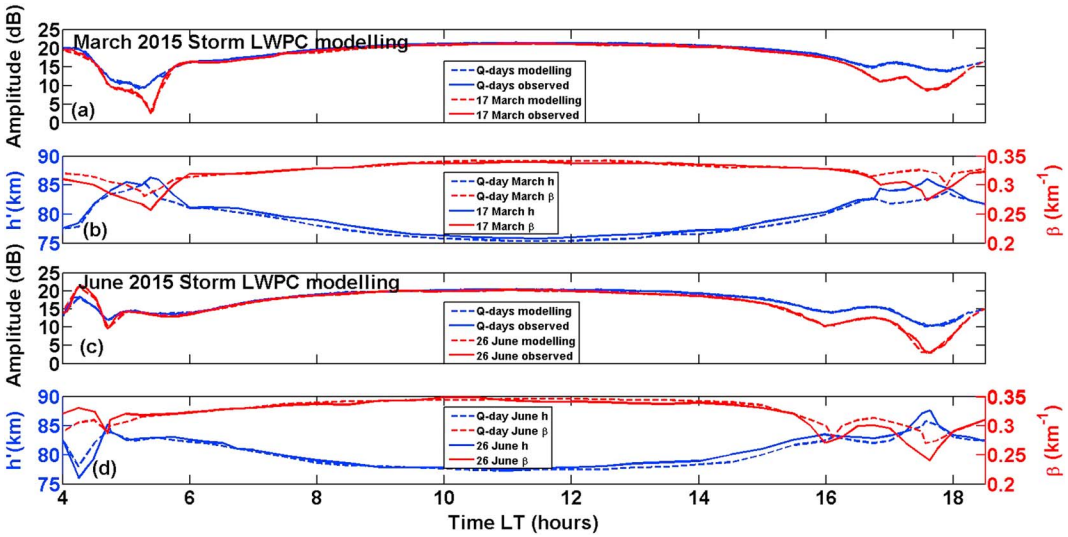

Figure 7. (a) Long-Wavelength Propagation Capability (LWPC) modeled amplitude (blue dashed line) and observed amplitude (blue solid line) for Q-day mean. The red dashed and solid lines give LWPC modeled amplitude and the observed amplitude for the storm day (17 March 2015). (b) The red dashed and solid lines show sharpness factor (β) for Q-day mean and for 17 March, respectively, and the blue dashed and solid lines show the reference height (h') for Q-day mean and for 17 March, respectively. (c and d) Variations of same parameters (amplitude, h', and β) for the June 2015 storm.

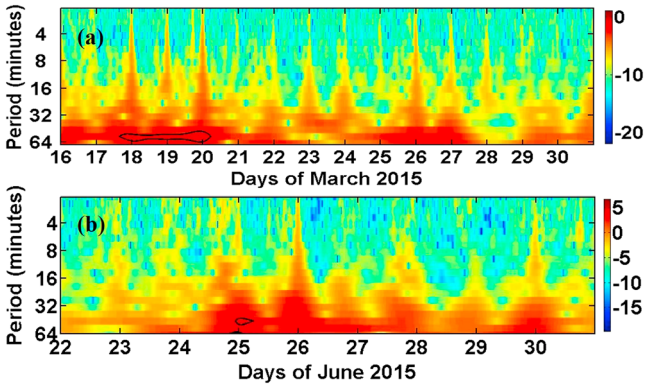

Figure 8. The wavelet spectra of NWC signal amplitude perturbation during the period 16–18 LT (evening terminator): (a) from 16–30 March for the March 2015 storm and (b) 22–30 June for the June 2015 storm.

times (when anomalies occurred) and the daylight portion of TRGCP. We have not modeled the signal for the nighttime of TRGCP due to large variability in the amplitude associated with nonstorm factors. The modeling results very closely reproduced the observed amplitude for *Q*-day mean and storm days with significant decrease in the amplitude during the ET both at minima1 and minima2 for both storms. The h' increased and β decreased during ET (minima1 and minima2) on storm days as compared to corresponding values of h' and β on *Q*-day mean, which gives a decrease in the *D* region electron density.

3.3. Mother Morlet Wavelet Signal Analysis

Using Mother Morlet wavelet technique (Mallat, 1998), we have analyzed the VLF signal amplitude during the March and June storms to look for possibility of presence of WLS associated with AGWs/TIDs (Sauli et al., 2006). We have first estimated the amplitude perturbation data for each day by finding an amplitude difference between mean of 5 *Q* days and respective storm days. This removes most of the diurnal variation along with terminator time effect. Further, we have selected amplitude data between 16 LT to 18 LT near ET (as we observed amplitude decrease near ET at minima1 and mimina2) on each day from 16 to 30 March (for March storm) and between 15:40 LT and 18:00 LT during 22–30 June (for June storm). Figures 8a and 8b show wavelet spectra of NWC signal amplitude, during March and June storms, respectively. The WLS of short period between ~40 and 60 min were seen during 17–20 March 2015 for March 2015 storm (Figure 8, top). Similarly, for June 2015 storm WLS with period ~40–50 min were only seen on 25 June 2015.

4. Discussion

We have analyzed the effects of the 17–19 March 2015 (St Patrick's Day) geomagnetic storm, first severe geomagnetic storm of solar cycle 24, and of 22–25 June 2015 storm (second largest storm of solar cycle 24) on subionospheric VLF signal (NWC 19.8 kHz) with propagation direction in southeast to northwest covering low-equatorial region. The VLF signal anomalies have been used to estimate the *D* region changes along the propagation paths during the main and recovery phases of both the storms. Several studies have been carried out on the upper ionospheric effect of these storms globally (e.g., Astafyeva et al., 2016, 2018; Nava et al., 2016; Ramsingh et al., 2015; Verkhoglyadova et al., 2016), but none so far appears on the *D* region effects particularly at the low latitudes. Further, as each storm is unique in the sense that it is characterized by strength, shock impact orientation, and duration of southward IMF B_z, geoeffectiveness of these storms in terms of ionospheric response is also distinctive. Hence, the aim of this paper is to analyze the effects of two storms (March 2015 and June 2015) of almost similar intensity on low-equatorial ionospheric *D* region.

The VLF signal amplitude clearly decreased during ET at minima1 and minima2 starting from the main phase of March storm, whereas for June storm the decrease in signal was only seen during the recovery phase. The VLF signal amplitude decrease recovered in about 9 days after the main phase of the March storm, which is a day after storm recovery, whereas in case of June storm the amplitude decrease was observed only during recovery phase (25–26 June). The storm associated VLF anomaly of ~3.4 dB on 25 June (2 days after storm main phase) at minima2 by the June storm is almost same as that by the March storm (~3.6 dB on 19 March, 2 days after main phase). Araki (1974) analyzed the NWC VLF signal recorded in Japan and found anomalous phase variation at the nighttime during the main phase of two geomagnetic storms which he attributed to an increase in the *D* region reference height. The *D* region reference height variation under space weather conditions (flares and magnetic storms) has been reported in few previous works (e.g., Araki, 1974; Grubor et al., 2005; Kumar et al., 2015). The decrease and redistribution of *D* region electron density with altitude due to magnetic storm related processes makes upper boundary of the Earth-ionosphere waveguide more or less diffused and higher which also changes the vertical electron density gradient; as a result VLF waves have to penetrate further up/down into the ionosphere to get reflected, suffering more/less absorption with respect to normal conditions (Grubor et al., 2005; Kumar et al., 2015). An

increase in the *D* region reference height during the magnetic storms has also been suggested (Kumar et al., 2015; Peter et al., 2006).

In many previous works, three possible mechanisms have been proposed for ionospheric changes during geomagnetic storm. These are (1) the storm-induced EEP, (2) prompt penetration (PP) of the high-latitude/auroral electric fields to low latitudes, and (3) the storm-induced circulation of high-latitude gas with depleted [O]/[N2] ratio to low latitudes and TID/AGW propagation during the storm from high to low latitudes. The latter two mechanisms primarily operate in the *F* region ionosphere at middle and low latitudes but have also been used to explain *D* region changes during storm in view of coupling between upper and lower ionospheres due to upper ionospheric $\mathbf{E} \times \mathbf{B}$ drifts. Ohya et al. (2006) suggested coupling between upper and lower ionospheric (*D* region) plasma during the great geomagnetic storm ($Dst = -182$ nT) of October 2000 due to storm associated change in the $\mathbf{E} \times \mathbf{B}$ plasma drift. They have estimated *D* region VLF reflection height using ELF-VLF tweek radio atmospherics recorded at low latitude to midlatitude station in Japan and compared it with *F* region virtual height ($h'F$) derived from ionosonde data. They found lowering/rising of *D* region VLF reflection height associated with increase/decrease in $h'F$. The high and midlatitude *D* region has been reported to be disturbed due to storm-induced EEP, which increases electron density in the localized *D* region (Cherniak & Zakharenkova, 2016; Jacobsen & Andalsvik, 2016; Voss et al., 1998). Peter et al. (2006) found a decrease in the VLF signal amplitude recorded in the midlatitude American sector for a great "Halloween storm" of October 2003 associated with EEP into the upper atmosphere. Bozoki et al. (2017) studied the effect of intense EEP observed by GOES and POES satellites during the St. Patrick's Day geomagnetic storm of 17–19 March 2015 on Schumann resonance (SR) intensity from high (polar) to lower latitudes SR stations. Their initial analysis suggested highest variation of SR intensity at the polar stations. Though the intensity decreased with decreasing latitude with larger at the middle-high latitude SR stations, low-latitude SR stations showed no effect. The NWC-Allahabad TRGCP (low-equatorial path) is such that EEP effect is very unlikely as already discussed in previous works (e.g., Bozoki et al., 2017; Kumar et al., 2015; Voss et al., 1998).

The PP electric field can arrive at low latitudes promptly within few minutes of main phase onset, and effect could be identified by sudden change in the signal strength. We did not observe sudden decrease in the VLF signal amplitude (Figures 3 and 5); rather amplitude decreased gradually starting during the main phase (~11 UT for NWC signal for March storm) and for June storm effect is only seen during recovery phase. Further, effect of PP electric field lasts for short duration only (about an hour or half), but in our case, ET time amplitude decrease was longer than 2 hr on 17 March, which occurred for several days during ET following the storm main phase day with decreased magnitude and duration. Therefore, PP electric field might have initial effect on the *D* region ionization via change in the *F* region $\mathbf{E} \times \mathbf{B}$ drifts through upper and lower ionosphere coupling. The St. Patrick's Day geomagnetic storm of 17–19 March 2015 as reported in many previous works showed *F* region positive storm effect in the Asian Sector (Astafyeva et al., 2015; Nava et al., 2016) including the Indian sector (Ramsingh et al., 2015; Tulasi Ram et al., 2015). Similarly, for 22–25 June storm Astafyeva et al. (2018) also found positive storm effect during the main phase over low latitude Asia sector. In our study of the storm effect in the *D* region in low-equatorial latitude using VLF measurements and LWPC modeling, we estimated a decrease in the electron density (negative storm effect) during main phase and recovery phase of March storm and during recovery phase for June storm, which could be understood by a change in the $\mathbf{E} \times \mathbf{B}$ drift. In order to understand the storm effect on *D* and *F* region plasma we have also plotted f_oF_2 data for both storms as shown in the Figure 9 (top and bottom) over the Allahabad station. Figure 9 shows that the *F* region critical frequency, f_oF_2 (which is an indication of peak electron density of F_2 region), over Allahabad station decreased during the main phase of both March and June 2015 storms. However, f_oF_2 data are missing for a few days during the main phase onset of these storms due to technical problems. The decrease in f_oF_2 during the recovery phase of the March 2015 storm could be attributed to the disturbance dynamo electric field effects changing the normal electrodynamics and to the storm-induced circulation of gas with depleted [O]/[N2] from high to the low latitudes that changes the composition of upper ionosphere. During the June 2015 storm, additionally, prompt penetrating electric fields associated with southward turnings of IMF B_z appear to have initiated the large decrease in f_oF_2 during the main phase of the storm. During the main phase of this storm, IMF B_z sharply turned southward at 19:20 UT (-37 nT) on 22 June and turned northward after about 30 min and again on 23 June IMF B_z turned southward at ~01:50 UT and remained largely negative (-25 nT) until ~06 UT (Astafyeva et al., 2016). The modeling results of Figures 4 and 6 along

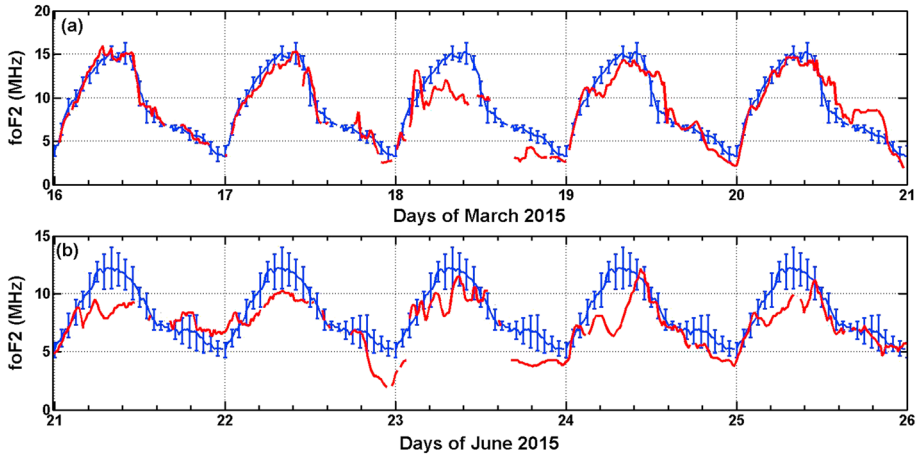

Figure 9. (a) The variation of f_oF_2 variation over Allahabad station during 16–21 March 2015 (red line). The blue line with error bar shows the mean f_oF_2 for 10 quiet days, and (b) shows the variations of f_oF_2 during 21–26 June 2015. The *x* axis represents the days of months with time in UT.

with Figure 9 indicate that the entire low-latitude ionosphere was affected in terms of decreasing the electron density under these storms.

The interesting point is long duration effect in the *D* region as compared to that in the *F* region; for example, here decrease in the amplitude during minima1 and minima2 of NWC signals for March storm appeared on several days during and about 1 day after the storm recovery. This is also known as "storm after effect" or long duration recovery of VLF signal anomaly. King and Fooks (1968) from analysis of effect of eight geomagnetic storms for the short path (~600 km) on LF (245 kHz) signal amplitude in the midlatitude region found that storm effect could last up to about 8 days. Spjeldvik and Thorne (1975) suggested that precipitation loss during the storm recovery is the major sources of the storm effect recovery at midlatitude with enhanced *D* region ionization persisting for a few days following the storm. Kumar et al. (2015) from the analysis of effect of intense 14–16 December 2006 geomagnetic storm on purely low-latitude VLF propagations (NWC and NPM to Suva, Fiji) suggested that *D* region composition perturbations recover slowly resulting in a long duration of VLF signal recovery in the low-latitude region. Kumar et al. (2015) observed long duration (for about 46 hr) of continuous decrease in the daytime signal strength of the NWC and NPM signals to low-latitude station, Suva, Fiji, whereas for this storm we observed short duration (about 2 hr) decrease in signal strengths during ET but appeared for several days following the storm onset day. Our observations are also supported by some previous works (e.g., Bolerose & Thomas, 1968; King & Fooks, 1968) that observed pronounced VLF effect during evening twilight. Interestingly, we do not observe "storm after effect" during June storm.

The third important mechanism for *D* region electron density variation is suggested through the Joule heating in the auroral region that generates AGWs which can propagate from high latitude to middle and low latitudes or even to the equatorial latitudes (Hunsucker, 1982; Laštovička, 2002). Such claims need direct observation of WLS in the *D* region. In order to see the presence of TIDs/AGWs during March 2015 and June 2015 storms, we have carried out the mother wavelet analysis of VLF signal amplitude during both the storms to look for WLS which are signatures of TIDs/AGWs (Mallat, 1998; Maurya et al., 2014; Sauli et al., 2006). The wavelet analysis of NWC signal amplitude at Allahabad (Figure 8) shows the existence of WLS at *D* region altitude with period between ~40 and 60 min for both the storms. Ramsingh et al. (2015) for low-equatorial latitude stations in the Indian sector at *F* region altitude reported AGWs signatures in the thermosphere meridional neutral winds. They also reported the presence of TIDs during recovery phase propagating from high latitude to low latitude. Yao et al. (2016) using TEC data analysis reported the presence of three TID events at different times during main phase of the March 2015 storm. They suggested that an equatorward surge of TIDs from high latitude could be largely due to AGWs excited by the March 2015 storm at *F* region altitudes. Thus, it is clear that the AGWs were present during the 17–19 March 2015 storm in the low-equatorial region. Further, we do not find any previous work as per our knowledge during the June storm showing AGWs signature in any region of ionosphere. The large variations in the *AE* index indicate Joule

heating in the Auroral region. The *AE* variation during both storms is shown in the Figures 1b and 1c (dark green line). The red circles mark the duration of large (~1,000 nT) variation in *AE* index. For March 2015 storm, a significant *AE* index variation is seen during 17–19 March and on 22 March, and for June 2015 storm, significant *AE* variation is seen during 22–23 June and on 25 June. Remarkably, our wavelet analysis result also shows presence of WLS with period between ~40 and 60 min on those days when *AE* index showed significant variations (i.e., 18–19 March and 25 June). Hence, wavelet analysis of the signal amplitude gives signatures of AGWs in the *D* region for both the storms. However, all the events of significant *AE* index variation did not show WLS events, which is probably due to factors (e.g., background wind and temperature) that affect the propagation of AGWs from high/auroral latitude to low latitude region (Cowling et al., 1971). The assumption of background winds was also supported by findings of Kumar et al. (2015). Kumar et al. (2015) by using wavelet analysis for NWC and NPM signals to low-latitude station, Suva, Fiji, did not find any signatures of wave-like activity. They also suggested that propagation of AGWs can be altered by background wind. Overall, it appears more reasonable that storm-induced AGWs/TIDs are responsible for *D* region composition changes associated with this storm.

The effects of both the geomagnetic storms were mainly observed during ET (minima1 and minima2). The minima (fadings) occur due to destructive interference of day and nighttime modes at the receiver, and depth of minima depends upon the intensity of destructive interference. The storm-induced change in the *D* region composition/ionization changes the VLF reflection height, hence the signal amplitude during day and nighttime and the depth of minima during terminator transition. No observation of storm associated amplitude anomalies during daytime (7–15 LT) indicates that the storm-induced change in the ionization was masked by the normal daytime increase in the ionization. The nighttime amplitude anomalies are not clearly detectable due to large nighttime variability of the *D* region (Maurya et al., 2012). At the time of morning terminator most of the path is in nightside; therefore, morning minima are highly variable to detect signal anomaly as compared to evening minima.

5. Summary and Conclusions

The first comprehensive analysis (observations and modeling) of the effects of the St Patrick's Day geomagnetic storm (17–19 March 2015) and 22–25 June 2015 storm on the *D* region ionosphere using VLF observations is presented. These storms with $Dst = -223$ nT and -204 nT were most intense space weather event of solar cycle 24. The VLF signal from transmitter NWC (19.8 kHz, Australia) covering low-equatorial low-latitude region was recorded at an Indian low latitude station, Allahabad. The main finding is that both storms showed significant decrease in the NWC signal strength near the ET time, which varied differently for both storms. For the March 2015 storm, NWC signal amplitude decreased starting from main phase on 17 March until 27 March, which is about 1 day after the storm recovery. For the June 2015 storm, the amplitude decrease was only seen on 2 days, 25–26 June during recovery phase, and no "storm after effect" was seen. The reduction in the amplitude occurred only near ET (minima1 and minima2) for both storms on the NWC signal. The LWPC modeling of signal anomaly gives an increase in the h' and a decrease in the β associated with a decrease in the *D* region electron density during storm main phase which recovered slowly. The morelet wavelet analysis of NWC signal amplitude showed the presence of WLS with a period of ~40–60 min near ET during both storms which are the signature of AGWs/TIDs at low latitudes associated with these storms. This is the first determination of AGWs in the equatorial to low-latitude *D* region ionosphere associated with the high latitude joule heating due to strong geomagnetic storms.

Acknowledgments
The author A.K.M. thanks the Science and Education Research Board (SERB) for financial support under Ramanujan Fellowship (file SB/S2/RJN-052/2016) and the Faculty Recharge Program (FRP) of the University Grants Commission (UGC) (ID FRP62343), New Delhi. The authors from Indian Institute of Geomagnetism (IIG) are grateful to the Department of Science and Technology, New Delhi, India, for support to carry out the project and work. The VLF and Ionosonde data set used in the present work is from Indian Institute of Geomagnetism (http://iigm.res.in/) operated AWESOME VLF recording instrument and Canadian Advanced Digital Ionosonde ionosonde located at Allahabad, India. The author (S.K.) thanks University of the South Pacific, Fiji, for financial support under Strategic Research Themes (SRT 2016) for a project grant on Natural Hazards study using VLF radio wave technique. The source of geomagnetic conditions used is from http://www.spaceweather.com/ and http://wdc.kugi.kyoto-u.ac.jp/.

References

Araki, T. (1974). Anomalous phase changes of trans-equatorial VLF radio waves during geomagnetic storms. *Journal of Geophysical Research: Space Physics*, *79*(31), 4811–4816. https://doi.org/10.1029/JA079i031p04811

Astafyeva, E., Zakharenkova, I., & Alken, P. (2016). Prompt penetration electric fields and the extreme topside ionospheric response to the 22–23 June 2015 geomagnetic storm as seen by the Swarm constellation. *Earth, Planets and Space*, *68*(1), 152. https://doi.org/10.1186/s40623-016-0526-x

Astafyeva, E., Zakharenkova, I., & Förster, M. (2015). Ionospheric response to the 2015 St. Patrick's Day storm: A global multi-instrumental overview. *Journal of Geophysical Research: Space Physics*, *120*, 9023–9037. https://doi.org/10.1002/2015JA021629

Astafyeva, E., Zakharenkova, I., Hozumi, K., Alken, P., Coïsson, P., Hairstonand, M. R., & Coley, W. R. (2018). Study of the equatorial and low-latitude electrodynamic and ionospheric disturbances during the 22–23 June 2015 geomagnetic storm using ground-based and space-borne techniques. *Journal of Geophysical Research: Space Physics*, *123*, 2424–2440. https://doi.org/10.1002/2017JA024981

Barr, R., Jones, D. L., & Rodger, C. J. (2000). ELF and VLF radio waves. *Journal of Atmospheric and Solar - Terrestrial Physics*, *62*(17-18), 1689–1718. https://doi.org/10.1016/S1364-6826(00)00121-8

Bolerose, J. S., & Thomas, L. (1968). Ionization changes in the middle latitude D-region associated with geomagnetic storms. *Journal of Atmospheric and Solar - Terrestrial Physics*, *30*, 1397–1413.

Bozoki, T. Sátori, G., Steinbach, P., Neszka, M., Mlynarczyk, J., Price, C., et al. (2017). Signature of St. Patrick geomagnetic storm on Schumann resonances, 19th EGU General Assembly (EGU2017) proceedings from the conference held 23–28 April, 2017, Vienna, Austria. (p. 1858).

Chakraborty, S., Sasmal, S., Basak, T., Ghosh, S., Palit, S., Chakrabarti, S. K., & Ray, S. (2017). Numerical modeling of possible lower ionospheric anomalies associated with Nepal earthquake in May, 2015. *Advances in Space Research*, *60*(8), 1787–1796. https://doi.org/10.1016/j.asr.2017.06.031

Cherniak, I., & Zakharenkova, I. (2016). Dependence of the high-latitude plasma irregularities on the auroral activity indices: A case study of 17 March 2015 geomagnetic storm. *Earth, Planets and Space*, *67*(1), 151–158. https://doi.org/10.1186/s40623-015-0316-x

Choudhury, A., De, B. K., Guha, A., & Roy, R. (2015). Long-duration geomagnetic storm effects on the D region of the ionosphere: Some case studies using VLF signal. *Journal of Geophysical Research: Space Physics*, *120*, 778–787. https://doi.org/10.1002/2014JA020738

Clilverd, M. A., Rodger, C. J., Gamble, R. J., Ulich, T., Raita, T., Seppälä, A., et al. (2010). Ground-based estimates of outer radiation belt energetic electron precipitation fluxes into the atmosphere. *Journal of Geophysical Research*, *115*, A12304. https://doi.org/10.1029/2010JA015638

Clilverd, M. A., Rodger, C. J., Thomson, N. R., Lichtenberger, J., Steinbach, P., Cannon, P., & Angling, M. J. (2001). Total solar eclipse effects on VLF signals: Observation and modeling. *Radio Science*, *36*(4), 773–788. https://doi.org/10.1029/2000RS002395

Clilverd, M. A., Thomson, N. R., & Rodger, C. J. (1999). Sunrise effects on VLF signals propagating over a long north-south path. *Radio Science*, *34*(4), 939–948. https://doi.org/10.1029/1999RS900052

Cohen, M. B., Inan, U. S., & Paschal, E. W. (2010). Sensitive broadband ELF/VLF radio reception with the AWESOME instrument. *IEEE Transactions on Geoscience and Remote Sensing*, *48*(1), 3–17. https://doi.org/10.1109/TGRS.2009.2028334

Cowling, D. H., Webb, H. D., & Yeh, C. K. (1971). Group rays of internal gravity waves in a wind-stratified atmosphere. *Journal of Geophysical Research*, *76*(1), 213–220. https://doi.org/10.1029/JA076i001p00213

Cummer, S. A., & Inan, U. S. (2000). Ionospheric E region remote sensing with ELF radio atmospherics. *Radio Science*, *35*(6), 1437–1444. https://doi.org/10.1029/2000RS002335

Ferguson, J. A. (1998). Computer programs for assessment of long-wavelength radio communications, Version 2.0: User's Guide and Source Files, No. TD-3030, Space and Naval Warfare Systems Center, San Diego, CA.

Grubor, D., Sulic, D., & Zigman, V. (2005). Influence of solar X-ray flares on the Earth -ionosphere waveguide. *Serbian Astronomical Journal*, *171*, 29–35.

Guha, A., De, B. K., Choudhury, A., & Roy, R. (2012). Spectral character of VLF sferics propagating inside the Earth ionosphere waveguide during two recent solar eclipses. *Journal of Geophysical Research*, *117*, A04305. https://doi.org/10.1029/2011JA017498

Hargreaves, J. K. (1992). *The solar-terrestrial environment*. New York: Cambridge University Press. https://doi.org/10.1017/CBO9780511628924

Hunsucker, R. D. (1982). Atmospheric gravity waves generated in the high-latitude ionosphere: A review. *Reviews of Geophysics*, *20*(2), 293–315. https://doi.org/10.1029/RG020i002p00293

Jacobsen, S., & Andalsvik, Y. L. (2016). Overview of the 2015 St. Patrick's Day storm and its consequences for RTK and PPP positioning in Norway. *Journal of Space Weather and Space Climate*, *6*, A9. https://doi.org/10.1051/swsc/2016004

Kikuchi, T., & Evans, D. S. (1983). Quantitative study of substorm-associated VLF phase anomalies and precipitating energetic electrons on November 13, 1979. *Journal of Geophysical Research*, *88*, 871–880.

King, J. W., & Fooks, J. L. (1968). Long-lasting storm effects in the ionospheric D-region. *Journal of Atmospheric and Solar - Terrestrial Physics*, *30*(4), 639–643. https://doi.org/10.1016/0021-9169(68)90066-4

Kleimenova, N. G., Kozyreva, O. V., Rozhnoy, A. A., & Soloveva, M. S. (2004). Variations in the VLF signal parameters on the Australia-Kamchatka radio path during magnetic storms. *Geomagnetism and Aeronomy*, *44*, 354–361.

Kumar, S., Kumar, A., Menk, F., Maurya, A. K., Singh, R., & Veenadhari, B. (2015). Response of the low-latitude D region ionosphere to extreme space weather event of 14–16 December 2006. *Journal of Geophysical Research: Space Physics*, *120*, 788–799. https://doi.org/10.1002/2014JA020751

Kumar, S., NaitAmor, S., Chanrion, O., & Neubert, T. (2017). Perturbations to the lower ionosphere by tropical cyclone Evan in the South Pacific region. *Journal of Geophysical Research: Space Physics*, *122*, 8720–8732. https://doi.org/10.1002/2017JA024023

Laštovička, J. (2002). Monitoring and forecasting ionospheric space weather effects of geomagnetic storms. *Journal of Atmospheric and Solar - Terrestrial Physics*, *64*(5-6), 697–705. https://doi.org/10.1016/S1364-6826(02)00031-7

Mallat, S. (1998). *A wavelet tour of signal processing*. San Diego, CA: Academic Press.

Marubashi, K., Cho, K. S., Kim, R. S., Kim, S., Park, S. H., & Ishibashi, H. (2016). The 17 March 2015 storm: The associated magnetic flux rope structure and the storm development. *Earth, Planets and Space*, *68*(1), 173–184. https://doi.org/10.1186/s40623-016-0551-9

Maurya, A. K., Phanikumar, D. V., Singh, R., Kumar, S., Veenadhari, B., Kwak, Y.-S., et al. (2014). Low-mid latitude D region ionospheric perturbations associated with 22 July 2009 total solar eclipse: Wave-like signatures inferred from VLF observations. *Journal of Geophysical Research: Space Physics*, *119*, 8512–8523. https://doi.org/10.1002/2013JA019521

Maurya, A. K., Veenadhari, B., Singh, R., Kumar, S., Cohen, M. B., Selvakumaran, R., et al. (2012). Nighttime D region electron density measurements from ELF-VLF tweek radio atmospherics recorded at low latitudes. *Journal of Geophysical Research*, *117*, A11308. https://doi.org/10.1029/2012JA017876

Nava, B., Rodríguez-Zuluaga, J., Alazo-Cuartas, K., Kashcheyev, A., Migoya-Orué, Y., Radicella, S. M., et al. (2016). Middle- and low-latitude ionosphere response to 2015 St. Patrick's Day geomagnetic storm. *Journal of Geophysical Research: Space Physics*, *121*, 3421–3238. https://doi.org/10.1002/2015JA022299

Ohya, H., Nishino, M., Murayama, Y., Igarashi, K., & Saito, A. (2006). Using tweek atmospherics to measure the response of the low-middle latitude D-region ionosphere to a magnetic storm. *Journal of Atmospheric and Solar - Terrestrial Physics*, *68*(6), 697–709. https://doi.org/10.1016/j.jastp.2005.10.014

Ohya, H., Shiokawa, K., & Miyoshi, Y. (2011). Long term variations in tweek reflection height in the D and lower E-regions of the ionosphere. *Journal of Geophysical Research*, *116*, A10322. https://doi.org/10.1029/2011JA016800

Peter, W. B., Chevalier, M. W., & Inan, U. S. (2006). Perturbations of mid-latitude subionospheric VLF signals associated with lower ionospheric disturbances during major geomagnetic storms. *Journal of Geophysical Research*, *111*, A03301. https://doi.org/10.1029/2005JA011346

Phanikumar, D. V., Kwak, Y.-S., Patra, A. K., Maurya, A. K., Singh, R., & Parke, S.-M. (2014). Response of the mid-latitude D-region ionosphere to the total solar eclipse of 22 July 2009 studied using VLF signals in South Korean peninsula. *Advances in Space Research*, *54*(6), 961–968. https://doi.org/10.1016/j.asr.2014.06.005

Ramsingh, S., Sripathi, S., Sreekumar, S., Banola, K., Emperumal, P. T., & Kumar, B. S. (2015). Low-latitude ionosphere response to super geomagnetic storm of 17/18 March 2015: Results from a chain of ground based observations over Indian sector. *Journal of Geophysical Research: Space Physics*, *120*, 10,864–10,882. https://doi.org/10.1002/2015JA021509

Ray, S., Roy, B., Paul, K. S., Goswami, S., Oikonomou, C., Haralambous, H., et al. (2017). Study of the effect of 17–18 March 2015 geomagnetic storm on the Indian longitudes using GPS and C/NOFS. *Journal of Geophysical Research: Space Physics*, *122*, 2551–2563. https://doi.org/10.1002/2016JA023127

Rodger, C. J., Clilverd, M. A., Thomson, N. R., Gamble, R. J., Seppälä, A., Turunen, E., et al. (2007). Radiation belt electron precipitation into the atmosphere: Recovery from a geomagnetic storm. *Journal of Geophysical Research*, *112*, A11307. https://doi.org/10.1029/2007JA012383

Sauli, P., Abry, P., Boska, P., & Duchayne, L. (2006). Wavelet characterization of ionospheric acoustic and gravity waves occurring during solar eclipse of August 11, 1999. *Journal of Atmospheric and Solar - Terrestrial Physics*, *68*(3-5), 586–598. https://doi.org/10.1016/j.jastp.2005.03.024

Selvakumaran, R., Maurya, A. K., Gokani, S. A., Veenadhari, B., Kumar, S., Venkatesham, K., et al. (2015). Solar flares induced D-region ionospheric and geomagnetic perturbations in the Indian sector. *Journal of Atmospheric and Solar - Terrestrial Physics*, *123*, 102–112. https://doi.org/10.1016/j.jastp.2014.12.009

Singh, R., Veenadhari, B., Cohen, M. B., Pant, P., Singh, A. K., Maurya, A. K., et al. (2010). Initial results from AWESOME VLF receivers: Set up in low latitude Indian regions under IHY2007/UNBSSI. *Current Science*, *98*(3), 398–405.

Spjeldvik, W. N., & Thorne, R. M. (1975). The cause of storm after effects in the middle latitude D-region. *Journal of Atmospheric and Terrestrial Physics*, *37*(5), 777–795. https://doi.org/10.1016/0021-9169(75)90021-5

Thomson, N. R., Clilverd, M. A., & Rodger, C. J. (2014). Low-latitude ionospheric D region dependence on solar zenith angle. *Journal of Geophysical Research: Space Physics*, *119*, 6865–6875. https://doi.org/10.1002/2014JA020299

Thomson, N. R., & McRae, W. M. (2009). Nighttime ionospheric D region: Equatorial and non equatorial. *Journal of Geophysical Research*, *114*, A08305. https://doi.org/10.1029/2008JA01400

Thomson, N. R., Rodger, C. J., & Clilverd, M. A. (2005). Large solar flares and their ionospheric D region enhancements. *Journal of Geophysical Research*, *110*(A9), 6306. https://doi.org/10.1029/2005JA011008

Thomson, N. R., Rodger, C. J., & Dowden, R. L. (2004). Ionosphere gives size of greatest solar flare. *Geophysical Research Letters*, *31*, L06803. https://doi.org/10.1029/2003GL019345

Tulasi Ram, S., Yokoyama, T., Otsuka, Y., Shiokawa, K., Sripathi, S., Veenadhari, B., et al. (2015). Dusk side enhancement of equatorial zonal electric field response to convection electric fields during the St. Patrick's Day storm on 17 March 2015. *Journal of Geophysical Research: Space Physics*, *121*, 538–548. https://doi.org/10.1002/2015JA021932

Verkhoglyadova, O. P., Tsurutani, B. T., Mannucci, A. J., Mlynczak, M. G., Hunt, L. A., Paxton, L. J., & Komjathy, A. (2016). Solar wind driving of ionosphere-thermosphere responses in three storms near St. Patrick's Day in 2012, 2013, and 2015. *Journal of Geophysical Research: Space Physics*, *121*, 8900–8923. https://doi.org/10.1002/2016JA022883

Voss, H. D., Walt, M., Imhof, W. L., Mobilia, J., & Inan, U. S. (1998). Satellite observations of lightning-induced electron precipitation. *Journal of Geophysical Research*, *103*, 11,725–11,744.

Wait, J. R., & Spies, K. P. (1964). Characteristics of the Earth-ionosphere waveguide for VLF radio waves, Tech. Note 300, Natl. Bur. of Stand., Boulder, CO.

Wu, C. C., Liou, K., Lepping, R. P., Hutting, L., Plunkett, S., Howard, R. A., & Socker, D. (2016). The first super geomagnetic storm of solar cycle 24: "The St. Patrick's Day event (17 March 2015)". *Earth, Planets and Space*, *68*(1), 151–163. https://doi.org/10.1186/s40623-016-0525-y

Yao, Y., Liu, L., Kong, J., & Zhai, C. (2016). Analysis of the global ionospheric disturbances of the March 2015 great storm. *Journal of Geophysical Research: Space Physics*, *121*, 12,157–12,170. https://doi.org/10.1002/2016JA023352

Zhang, S.-R., Zhang, Y., Wang, W., & Verkhoglyadova, O. P. (2017). Geospace system responses to the St. Patrick's Day storms in 2013 and 2015. *Journal of Geophysical Research: Space Physics*, *122*, 6901–6906. https://doi.org/10.1002/2017JA024232